European Research Infrastructure supporting Smart Grid and Smart Energy Systems Research, Technology Development, Validation and Roll Out – Second Edition

Project Acronym: **ERIGrid 2.0**

Project Number: **870620**

Technical Report Lab Access User Project

Dynamic Characterization of Power-Electronics-based-Microgrid (Dyn-PEM)

Access Duration: 08/11/2022 to 17/11/2022

Funding Instrument:	Research and Innovation Action
Call:	H2020-INFRAIA-2019-1
Call Topic:	INFRAIA-01-2018-2019 Integrating Activities for Advanced Communities
Project Start:	1 April 2020
Project Duration:	54 months
User Group Leader:	Salman Harasis (TTU)

This project has received funding from the European Union'sHorizon 2020 research and innovation programme under Grant Agreement No. 870620.

Report Information

Document Administrative Information	
Project Acronym:	ERIGrid 2.0
Project Number:	870620
Access Project Number:	[nnn]
Access Project Acronym:	[Dyn-PEM]
Access Project Name:	[Dynamic Characterization of Power-Electronics-based-Microgrid]
User Group Leader:	[Name of Lab Access User Group Leader (institution name)]
Document Identifier:	ERIGrid2-Report-Lab-Access-User-Project-AccessProjectAcronym-draft-vn.n
Report Version:	vn.n
Contractual Date:	dd/mm/yyyy
Report Submission Date:	dd/mm/yyyy
Lead Author(s):	Dr.Salman Harasis (TTU)
Co-author(s):	Dr. Abdulla Eial Awwad (TTU)
Keywords:	Distribution networks, Distributed energy resources, European Union (EU), H2020,Project, ERIGrid 2.0, GA 870620
Status:	x draft, final

Change Log

Date	Version	Author/Editor	Summary of Changes Made
dd/mm/yyyy	v1.0	Salman Harasis (TTU)	Draft report template

Table of Contents

List of Abbreviations

EC	European Commission
LA	Lab Access
BES	Battery energy storage
DG	Diesel Generator
DER	Distributed Energy Resource
FFR	Fast frequency response
GFD	Grid feeding
GFM	Grid forming
H	The inertia constant
HIL	Hardware-in-the-loop
kW	kilowatt
MPPT	maximum power point tracking
PFR	primary frequency response
PV	photovoltaics
RoCoF	rate of change of frequency
UFLS	under-frequency load shedding

Executive Summary

The concept of Microgrid has been introduced as a power generation platform for distributed generation (DG) where DERs are efficiently and reliably integrated. A standard feature of the Microgrid is the capability to work in islanding and grid-connected modes with minimal disruption for the permissible voltage and frequency tolerance levels [1, 2].

The growth of inverter-based Microgrids has expanded significantly in recent decades. The wide spread of Microgrid networks has provided better environmental and economic solutions over conventional power systems. The formation of distributed energy systems aims to enable the large-scale integration of renewable energy resources. However, there are many stability and control issues that need to be addressed to better stabilize and maturase the deployment of Microgrids as a next-generation power system.

In Microgrid applications, inertial response (IR) and fast frequency response (FFR) terminologies refer to the transient response of the power system caused by the kinetic energy stored in generators and in motors that are directly coupled to the grid. The fast frequency response is an indirect indicator to the amount of inertia available in the system under certain loading conditions. The purpose of the investigations is to measure and characterize the aforementioned terminologies.

During the 2-week access period, several successful experiments were carried out using RTDS power network emulator. The experiments were conducted, and the results were obtained, processed, and analyzed.

The primary goals and findings from the lab access are categorized as:

- Performing hardware real-time emulation of inverter-based DGS.
- Measuring and quantifying the equivalent inertia amount in the Microgrid composed of different inverter-based DERs.
- Evaluating the optimal mix of grid forming and grid feeding DGs using real-time measurements under dynamic operating conditions.

1 Lab-Access User Project Information

1.1 Overview

USER PROJECT	
User Project Acronym	Dyn-PEM
User Project Title	Dynamic Characterization of Power-Electronics-based-Microgrid
ERIGrid Reference	
ERIGrid 2.0 TA Call No.	1st call

HOST RESEARCH INFRASTRUCTURE			
Name	VTT Technical Research Centre of Finland Ltd		
Country	Finland		
Start date	08/11/2022	No. of access days	8
End date	17/11/2022	No. of stay days	10

USER GROUP	
Name (Leader)	Salman Harasis
Organization	Tafila Technical university (TTU)
Country	Jordan

1.2 Research Motivation, Objectives, and Scope

Our big motive behind the conducted research was to investigate and validate critical issues related to the reliability of renewables integration into Microgrid networks. The associated dynamics of the inverter-based DERs introduced by their unconventional dynamics are of interest in this research. Utilizing the host lab (i.e., VTT smart grid lab) capabilities and useful appliances to run the experiments in real time was necessary to arrive at accurate conclusions about the attained results. The objectives of the conducted experiments were to examine the dynamic operation of a Microgrid test-bench composed of several DERs that represent different types of energy sources. A specific Microgrid configuration that represents a complete system able to run autonomously without a utility interface is considered. Another major objective was to determine the optimal operating modes of the integrated DERs (grid feeding, grid forming, or VSG) under certain system configurations, load types, and types of running sources. The interaction between the disturbances and the implemented control strategy has been captured. For a specified capacity of the integrated DERs, the specific operating points of each one,

and the implemented control strategy, determining the FFR capability under transient conditions were successfully performed.

1.3 Structure of the Document

This document is organized as follows:

- Section 2 briefly outlines the state-of-the-art/state-of- technology that provides the basis of the realized Lab Access (LA) User Project (UP).
- Section 3 briefly outlines the performed experiments, whereas
- Section 4 summarizes the results and conclusions. Potential open issues and suggestions for improvements are discussed in Section 5.
- Finally, additional information is provided in Appendix A and B.

2 State-of-the-Art/State-of-Technology

2.1 Introduction

The Microgrid concept incorporates distributed generation (DG) with loads in a distribution system and is relatively new. In Microgrids, different types of energy sources (renewable and non-renewable) and energy storage systems (ESS) are combined to satisfy the demand for loads that can either be connected to the grid or operated in an island mode [3]. Recently, there has been an increase in the penetration of converter-interfaced generation, including photovoltaics (PVs) and wind, into power networks to replace conventional synchronous generators (SGs). According to IRENA, the total worldwide renewable power generation capacity, at the end of 2021, is 3064 GW. Solar and wind energy account for 54.6% of the total global renewable generation capacity, solar accounts for 849 GW (27.7%) and 825 GW (26.9%) for wind [4].

Numerous amounts of research have discussed the impact of integrating all types of inverter based DERs on the voltage and frequency profiles. However, few of them considered the whole system configuration, the types of the connected load, the optimal DG combination, and the exact amount of inertia levels. Furthermore, few of the papers reported in the literature show an adequate experimental validation to the obtained results. Frequency and RoCoF measurements have been done using different techniques with no specific standard. These, altogether, motivated us in this work to experimentally investigate Microgrid frequency profile under several operating conditions. Therefore, a mature large-scale proliferation of power-electronics-based-Microgrid network can be realized. In [1], the stabilized paralleling of a Microgrid with the utility has been investigated and the impact of reactive power sharing on the PLL control loop has been examined under different loading conditions. In [2], the authors related the amount of virtual inertia to the frequency response of the system under faulty conditions. The researchers in [5, 6], addressed the problem of fast frequency response in Microgrids with low inertia. A direct coupling between the frequency response and inertia level has been quantified without considering the system dynamics, load type, and the system parameters. The work done in [7] investigated the interaction between the secondary and primary control loops to stabilize the Microgrid operation.

With increases in computing power and accessible data processing, artificial intelligence techniques are offering much more efficient and powerful ways to handle the limitation of the conventional control techniques. The inclusion of hardware in the loop (HIL) in the grid system would introduce innovations and give new directions to the electrical grid. The advancement of cooperative controllers in enabling a simultaneous voltage and frequency

control boosts the processing speed and improves the reliability and efficiency. The researchers in [8–10] investigated the transient frequency stabilization under different operating scenarios and load models. In [10], the impact of controller gains on frequency and voltage profiles have been carefully investigated. Ref [11] discussed the implementation of real-time control of high-performance scheme for grid connected PV system. The controller is designed for power quality improvement based on model predictive control scheme optimized using PSO algorithm. The work presented in [12–14] focused on using different techniques to manage and control the inverter power flow, frequency, and voltage in Microgrid test benches.

Due to their variable speed operation capability, doubly fed induction generators (DFIGs) and permanent magnet synchronous generators (PMSGs) have been widely used in wind energy conversion systems (WECS). Both generators have spinning inertia, but this inertia is isolated by power converters [15]. In this context, the system inertia significantly reduces, resulting in a major challenge to maintaining system stability [16]. As the inertia decreases, the frequency deviations from the nominal value pose a significant issue [17, 18]. As a result, unintentional triggering of over/under frequency relays, load-shedding, and other effects may occur [19].

Considering abnormal grid conditions, the technical requirements for the frequency measurement are reviewed in [20]. An improved frequency measurement logic based on a phase-locked loop (PLL) using control hardware-in-the-loop (CHIL) is also presented. The authors in [21] present a methodology for modelling aggregated active behaviors of the primary frequency response. A supplementary control method for providing frequency support service from a wind energy conversion system (WECS) using an inertia controller (i.e., synthetic inertia) and droop controller is presented in [22]. A model for synthetic inertia for dynamic power system stability is presented in [23]. The model includes droop control with an inertial energy storage model and can be included as a supplementary control structure in wind turbine control models. The authors in [24] use a statistical method based on the synchronous and non-synchronous sources to quantify inertia in the network when inverters integration is increased. The spatial distribution of inertia is studied in [25], and a method for quantifying the inertial heterogeneity of a power system is evaluated. Furthermore, previous studies discussed different inertia estimation methodologies based on optimized power point tracking strategy [26], synchronous inertia and virtual inertia [27], synchrophasor measurement [28]. The benefits and drawbacks of various inertia estimate approaches are discussed in [19].

Different studies have been conducted to create control approaches for energy storage systems (EES) in order to offer FFR and increase power system inertia in order to secure frequency stability [29]. An optimized control strategy is investigated in [26] for primary

frequency regulation in large-scale power systems with a high level of wind energy penetration. Further, a computational approach was developed to investigate the locational effect of fast-frequency response-based grid-following converters and grid-forming converters [30].

Additionally, real-time simulation and the use of HIL capable simulators have proved beneficial in expectations of reactions to faults, disturbances, load changes, and protective measures [31, 32]. As a result, the behavior of systems may be accurately monitored, and faults can be addressed prior to field implementations as has been highlighted in [33, 34]. A detailed review of real-time modelling, control, and energy management techniques in Microgrids is presented in [35] wherein a summary of different applications of HIL in Microgrids based on their technology are compared and analyzed.

2.2 Inertia Variability

Typically, the numbers and types of sources run in power system vary in an uncertain manner depending on the connected load and some economic and technical reasons. This, in turn, causes a change in the available amount of inertia as illustrated in Fig. 1. In the conducted experiment, it has been shown that the total available inertia is dictated by control type of DER, size of connected dispatchable generator, and the amount of its inertia constant [19].

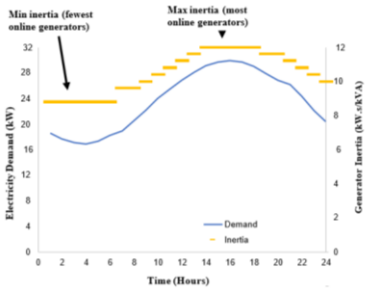

Fig. 1: dynamic inertia formulation

2.3 Maintaining Minimum Inertia for Reliable Microgrid Operation and Fast Frequency Response

Fast frequency response (FFR) illustrates the ability of DERs to increase the net supply of energy much faster than traditional mechanical-based [30]. FFR capability helps minimize the impact of low inertia as fast frequency drop that is caused by low inertia can be compensated by the fast response of FFR-enabled DER. As battery storage is rated for its capacity, its FFR capability is maximized where some battery types can increase their output power above the rated in just few cycles and change the mode from charging to discharging in very quick manner [6, 26].

The inverter-based DER provides frequency response can be synthesized where the electromechanical dynamic associated with synchronous generators have been replaced by sensors and control strategies that control the transient response of the DER, accordingly.

3 Executed Tests and Experiments

3.1 Test Plan, Standards, Procedures, and Methodology

The emulated Microgrid case is shown in Fig. 2 where BES, PV system, and DG are connected to utility grid through a transfer switch. The battery is characterized by its rated capacity in kWh, where the PV represents a variable source that has intermittent power output. The DG is a dispatchable generator that regulates the voltage and frequency under Microgrid autonomous mode of operation while supplies the required power according to its predetermined droop. The associated dynamics of this diversified mixture of generation is considered in this report.

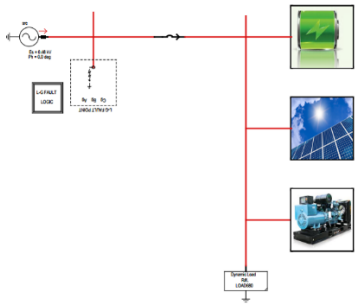

Fig. 2: The configuration of the Microgrid

The real time digital simulator (RTDS) is utilized to construct the Microgrid. The Microgrid is emulated according to HIL concept as illustrated in Fig. 3. Dedicated RSCAD® software was used to implement the system and communicate with hardware.

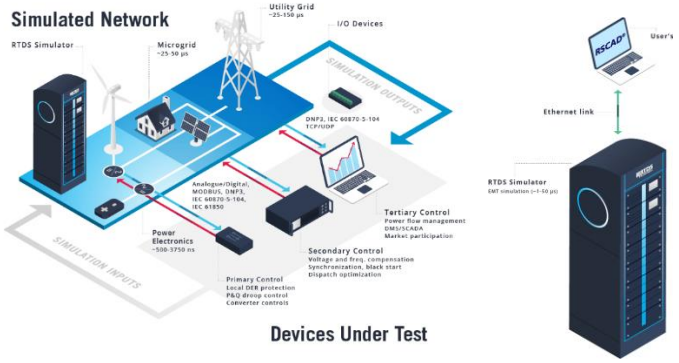

Fig. 3 The real-time emulated Microgrid using RTDS

Functions relevant to the operation of the system under test are:

- DERs with Q-V and P-f controllers.
- DERs works under different loading conditions (by having variable loads),
- DERs with their power/voltage/frequency are accessed to be measured. (Instantaneous current and voltage signals).

3.2 Test Plan and procedure

The cases investigated are summarized using the flowchart given in Fig. 4. The variable integration level is emulated using different solar insolation levels. The power sharing of the DG is adjusted according to its droop coefficient. The load is changed by switching parallel load banks.

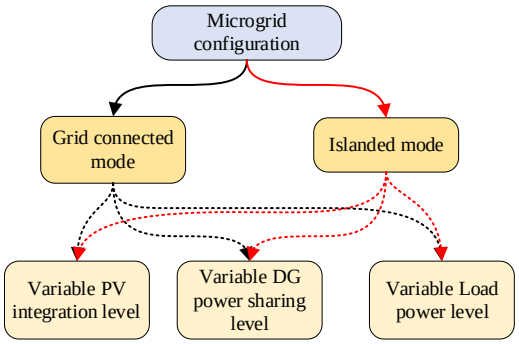

Fig. 4 the scenarios of microgrid configurations

According to the scenarios, the variables of the system are:

- The grid connection (grid connected, islanded)
- The PV insolation level (200, 400, 600, 800, 1000 w/m^2
- The amount of the connected load (0.5 pu, 1.0 pu, 1.3 pu).
- The droop coefficient of the DG (0.002-0.005 Hz/kW).
- The inertia of the DG

The control applied to each DER are:

PV: mppt-controlled DER

DG: dispatchable droop-controlled DER

BES: voltage-controlled DER (dispatchable)

Grid: isochronous controlled sources.

TIME SCHEDULE

Table I presents the schedule including setting up the lab appliances, preparing the required wiring, and configuring the emulated models.

Table I: Time Schedule

Week 1	08/11/2022	Kick-off meeting.
	09/11/2022	configuring the system and data acquisition
	10/11/2022	Building the system Performing Test-1
	11/11/2022	Performing Test-1 (Cont'd)
Week 2	14/11/2022	Preliminary results assessment of Test-1
	15/11/2022	Performing Test-2
	16/11/2022	Performing Test-3
	17/11/2022	Performing Test-3 for unstable cases

The Test Methodology

The methodology of the project is explained in three cascaded stages identified by specific tasks and objectives.

Stage-1: Configuring the Microgrid:

- The aim of this stage is to provide the required wiring and measuring instruments, configuring the Microgrid, and the necessary communications to start the initial functionality test.

Stage -2: Operating a Microgrid for inertia measurement:

- The aim of this stage is to develop simulated models of the system to assess the performance when integrated into the power grid under different operating conditions. The tasks associated with this stage are:
- Develop the hardware in the loop routines for low power testing and real time measurements.
- Invoke the simulated models of the DGs for real time testing/emulation.
- Initiate a generation side step-change / Initiate a load side step-change. (The test is repeated under different operating scenarios).
- Capture the effect of the DG control bandwidth on the FFR. (The cutoff frequency of the droop control LPF and the gains of SG).

3.3 Data Management and Processing

For each case study, the voltage, current, power, and frequency signals are obtained from the system according to the communication protocol configured in the RTDS. The signals are plotted using the dedicated RSCAD software and exported as a (.csv) files for signal processing. Fig. 5 shows the screenshot of the RSCAD interface used to emulate the Microgrid.

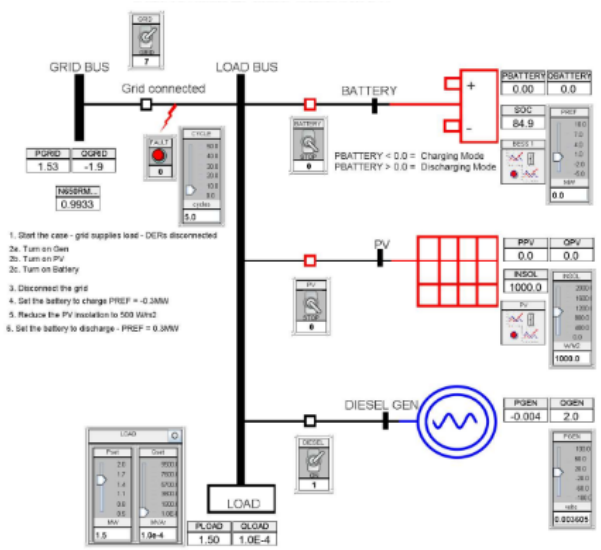

Fig. 5 the emulated Microgrid implemented in RSCAD

4. Results and Conclusions

As a result of the lab access, more than 20 test records were obtained. The cases were conducted under different configurations of the Microgrid. The events occurred in the system include load and generation side disturbances. The different configurations of the Microgrid are as follows.

- Configuration -1(grid connected mode): PV and DG are connected to the grid.
- Configuration -2 (grid connected mode): PV, DG, and BES are connected to grid under step load change.
- Configuration -3 (grid connected mode): PV and DG are connected to the grid under different PV integration levels.
- Configuration -4 (islanded mode): the DG runs as a grid forming DER, BES is voltage-controlled, and PV is MPPT controlled.

Part-1: Grid connected mode:

Several experiments were carried out when the Microgrid was connected to the utility grid. The major waveforms used in the analysis are reported in the following. The DG was deployed first work in parallel with the grid. After few seconds, the PV system is inserted. Fig. 6 to Fig. 11 show the frequency and power profiles of the load in second where the variation $+\Delta f, -\Delta f$, $+\Delta P, -\Delta P,$ and Δt for each frequency swing are calculated to determine H in each case.

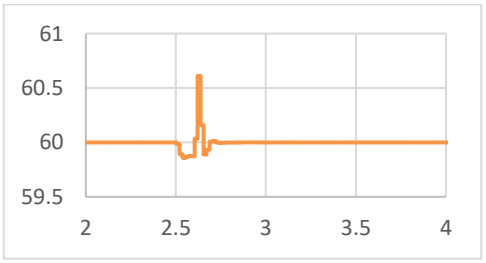

(a) the frequency profile

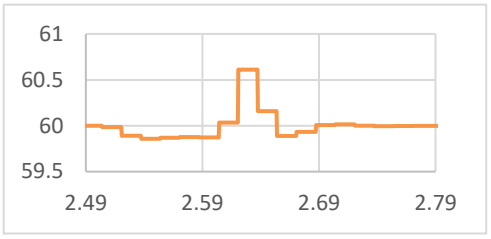

(b) Close-up view of the frequency

Fig 6: (Case-1) system frequency (Hz)

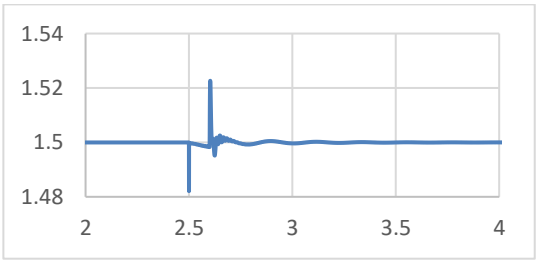

(a) the load power profile

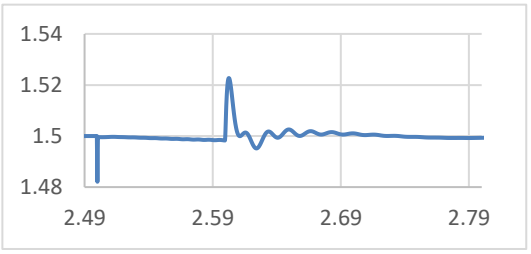

(c) Close-up view of the load power

Fig. 7: (Case-1) Load power (kW)

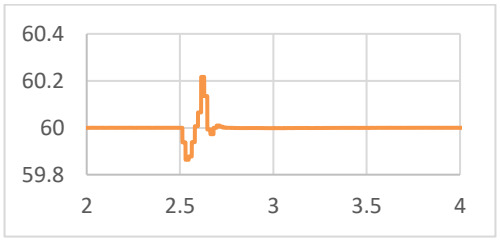

(a) the frequency profile

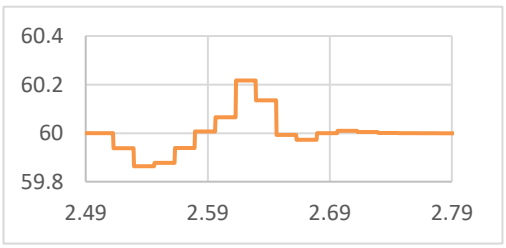

(b) Close-up view of the frequency

Fig. 8:(Case-2) system frequency (Hz)

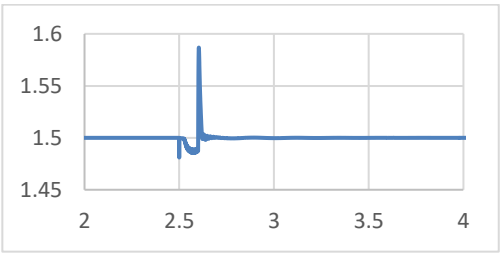

(a) the load power profile

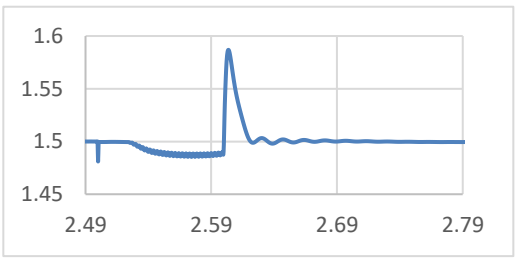

(b) Close-up view of the frequency

Fig. 9: (Case-2) Load power (kW)

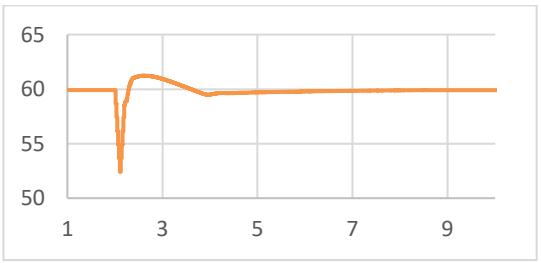

(a) the frequency profile

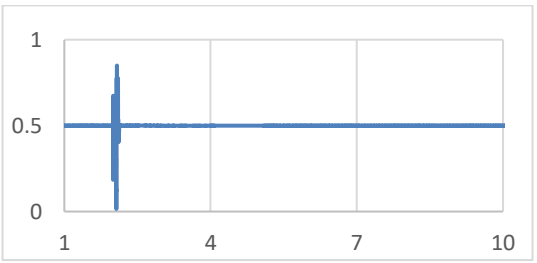

(a) the load power profile

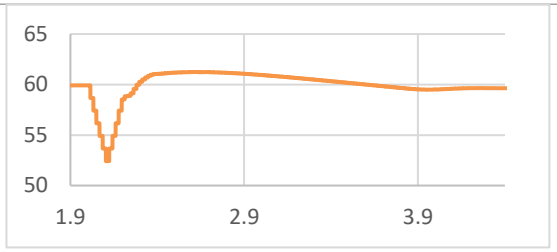

(b)Close-up view of the frequency

Fig. 10 :(Case-3) Load Freq (Hz)

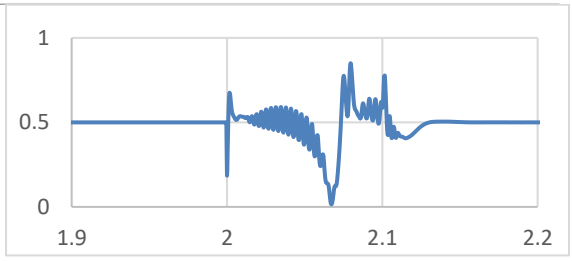

(b) Close-up view of the frequency

Fig. 11: (Case-3) Load power (kW)

Part-2: Islanded mode:

In this mode of operation, the DG is stabilizing the voltage and the frequency. The PV is interacting with the system using a PLL loop under MPPT control. The battery is dispatchable source works in voltage-controlled mode.

Additional cases were considered as given in Fig. 10 to Fig. 14 where the frequency dynamics were captured under different PV insolation levels and step load changes.

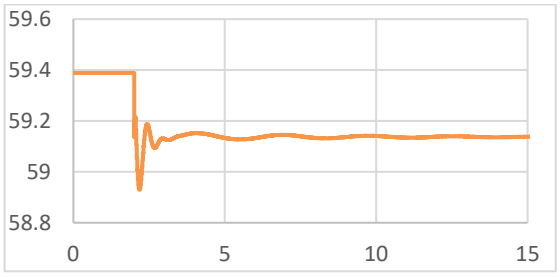

(a) the frequency profile

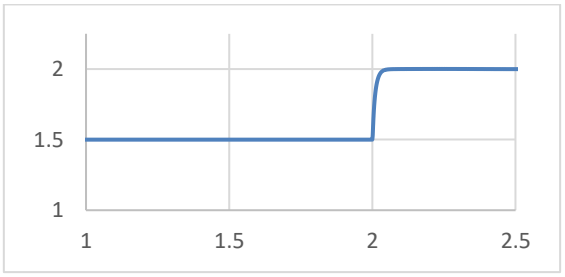

(b) the load power

Fig. 12: (case-4) : islanded microgrid under 25% load change and PV integration level-1

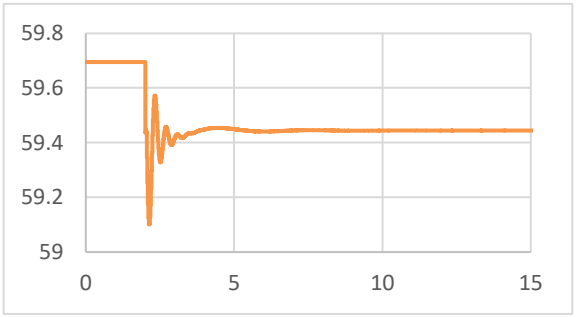

(a) the frequency profile

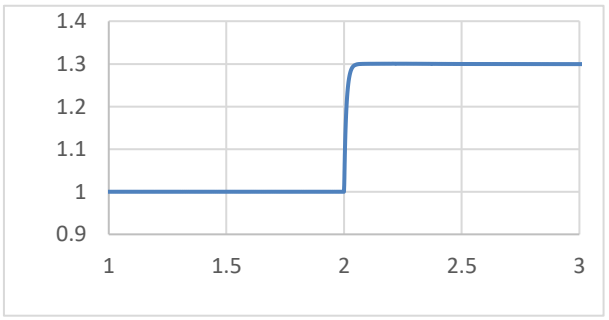

(b) the load power

Fig. 13: (Case-5) islanded microgrid under 30% and PV integration level-2

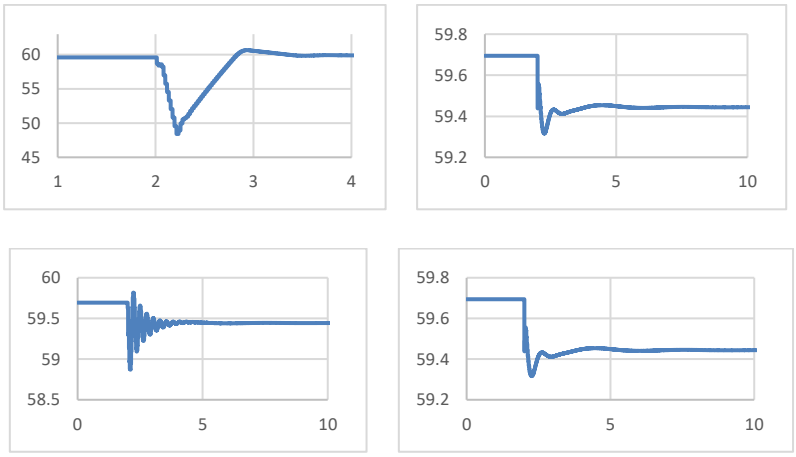

Fig. 14: the frequency dynamics under different step load changes

Unstable Islanded mode

The system was forced to run under unstable operating conditions to determine the critical level of inertia required to stabilize the microgrid. Fig. 15 shows some of these cases. However, the results concluded from these cases require further experimentation for reasonable critical inertia determination since many factors were found to be involved in this critical case.

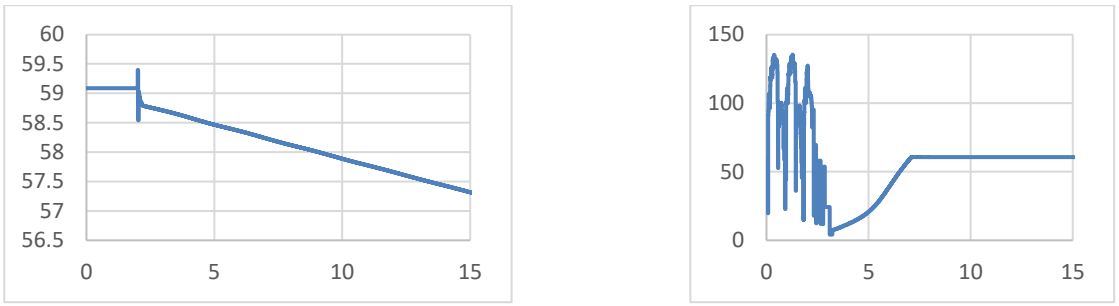

(a) unstable case-A (b) unstable case-B

Fig. 15 unstable frequency profiles occur due to large sudden load increase

The undamped natural frequency (ω_n) and the damping ratio (ζ) for the equivalent system's swing equation are also used to identify H. The derivation of the equations is carried out in appendix B.

$$\omega_n = \sqrt{\frac{EV\cos\alpha}{X}\frac{\omega}{2H}} \quad (1)$$

$$\zeta = \frac{D}{4H\omega_n} \quad (2)$$

Following the procedure deveolped in [19, 29], the value of **H** can be evaluated for each system conditions. The fomulation of the transient energy evolved in the system under any event yields the equivalent H given in (3). The equivalent inertia calculated using (3) shows small discrepency due to the approximation considerd in calualting the transient energy.

$$H_{eq} = \frac{\sum H_{SG_i} S_{B_i} + \sum H_{DER_j} S_{B_j}}{\sum S_{B_i} + \sum S_{B_j}} = 0.5 \frac{\omega_s^2}{S_{base}} \sum J_i \quad (3)$$

Table II: comaprative results of inertia determination methodologies

Case #	Estimated inertia constant (H_e) in kW.s/kVA	Calculated inertia constant (H_c) in kW.s/kVA	Error (%) $\left\|\frac{H_c - H_e}{H_c}\right\| * 100\%$
Case 1	≈2.21	2.30	3.9 %
Case 2	≈1.81	2.00	9.5%
Case 3	≈1.93	1.80	7.2%
Case 4	≈1.95	2.10	7.1%
*Other cases	≈2.66	2.40	10.8%

*(other cases): H was evaluated taking the average value of different cases where the system was running under different system configurations and loading scenarios.

The results show that there is an inevitable compromise between FFR and the required inertia level in the system, see Table II. This would provide a promising solution to rethink in deploying an enhanced GFD DERs in parallel with the GFM DERs. This conclusion may be strengthened by conducting more cases that include different voltage levels.

3.4 The impact of using the ERIGrid 2.0 Lab Access program

The opportunity given through the ERIGrid 2.0 Lab Access program and VTT lab made the dreams of the proposal come true. The answers to many research questions have been supported after conducting the experiment. Moreover, new research questions came across and added some research gaps to be answered in the next future.

3.5 Conclusions

Microgrid frequency drops dramatically if a sudden disturbance occurs in the system. This is due to the comparable load to generation capacity ratio. Inertia helps the system to resist the frequency drop, giving the primary control the time to react and balance the generation and load. Inertial response is one of the important criteria that help maintain the stability of the microgrid. Several experiments have been conducted to characterize the microgrid operation from the inertial response perspective. Inertia determination and quantification experimentation of the microgrid under study have been considered based on different operating scenarios.

4 Open Issues and Suggestions for Improvements

Additional research is needed to conduct in order to understand how to optimize the provision of FFR from to maximize its benefits in low inertia microgrids. Moreover, determining the critical value of the inertia constant in each microgrid requires deep investigations where overall system variables, nonlinearity, and fidelity to be considered for microgrid stability evaluation and maximizing the integration level of renewables.

References

[1] L. Huang *et al.,* “Grid-Synchronization Stability Analysis and Loop Shaping for PLL-Based Power Converters With Different Reactive Power Control,” *IEEE Trans. Smart Grid*, vol. 11, no. 1, pp. 501–516, 2020.

[2] Q. Peng, J. Fang, Y. Yang, T. Liu, and F. Blaabjerg, “Maximum Virtual Inertia From DC-Link Capacitors Considering System Stability at Voltage Control Timescale,” *IEEE J. Emerg. Sel. Topics Circuits Syst.*, vol. 11, no. 1, pp. 79–89, 2021, doi: 10.1109/JETCAS.2021.3049686.

[3] M. Shafiullah *et al.,* “Review of Recent Developments in Microgrid Energy Management Strategies,” *Sustainability*, vol. 14, no. 22, p. 14794, 2022, doi: 10.3390/su142214794.

[4] IRENA, *Renewable capacity highlights.* [Online]. Available: https://www.irena.org/ (accessed: Apr. 11 2022).

[5] B. Alghamdi and C. A. Canizares, “Frequency Regulation in Isolated Microgrids Through Optimal Droop Gain and Voltage Control,” *IEEE Trans. Smart Grid*, vol. 12, no. 2, pp. 988–998, 2021, doi: 10.1109/TSG.2020.3028472.

[6] U. Tamrakar, D. A. Copp, T. Nguyen, T. M. Hansen, and R. Tonkoski, “Optimization-Based Fast-Frequency Estimation and Control of Low-Inertia Microgrids,” *IEEE Trans. Energy Convers.*, vol. 36, no. 2, pp. 1459–1468, 2021, doi: 10.1109/TEC.2020.3040107.

[7] O. Babayomi, “Distributed Secondary Frequency and Voltage Control of Parallel-Connected VSCs in Microgrids: A Predictive VSG-Based Solution,” *CPSS TPEA*, vol. 5, no. 4, pp. 342–351, 2020, doi: 10.24295/CPSSTPEA.2020.00028.

[8] S. Yang-Wu *et al.,* “Load Frequency Control Strategy for Wind Power Grid-connected Power Systems Considering Wind Power Forecast,” in *2019 IEEE 3rd Conference on Energy Internet and Energy System Integration (EI2)*, Changsha,

China, 2019, pp. 1124–1128.
[9] A. Krama, L. Zellouma, B. Rabhi, S. Refaat, and M. Bouzidi, “Real-Time Implementation of High Performance Control Scheme for Grid-Tied PV System for Power Quality Enhancement Based on MPPC-SVM Optimized by PSO Algorithm,” *Energies*, vol. 11, no. 12, p. 3516, 2018, doi: 10.3390/en11123516.
[10] W. Mendieta and C. A. Canizares, “Primary Frequency Control in Isolated Microgrids Using Thermostatically Controllable Loads,” *IEEE Trans. Smart Grid*, vol. 12, no. 1, pp. 93–105, 2021, doi: 10.1109/TSG.2020.3012549.
[11] C. Lu, S. Guan, M. Yan, F. Zhang, K. Wu, and B. Wang, “Grid Connected Photovoltaic Power Generation Station and it's Influence on Dispatching Operation Mode,” in *2018 2nd IEEE Conference on Energy Internet and Energy System Integration (EI2)*, Beijing, 2018, pp. 1–4.
[12] S. Pal and K. B. Sahay, “Modeling of Solar Energy Grid Integration System Using Typhoon HIL,” in *2018 International Electrical Engineering Congress (iEECON)*, Krabi, Thailand, 2018, pp. 1–5.
[13] M. Jalali, V. Kekatos, N. Gatsis, and D. Deka, “Designing Reactive Power Control Rules for Smart Inverters Using Support Vector Machines,” *IEEE Trans. Smart Grid*, vol. 11, no. 2, pp. 1759–1770, 2020, doi: 10.1109/TSG.2019.2942850.
[14] S. Bhela, V. Kekatos, and S. Veeramachaneni, “Smart Inverter Grid Probing for Learning Loads: Part II—Probing Injection Design,” *IEEE Trans. Power Syst.*, vol. 34, no. 5, pp. 3537–3546, 2019, doi: 10.1109/TPWRS.2019.2906306.
[15] A. Eial Awwad, “Dynamic Performance Enhancement of a Direct-Driven PMSG-Based Wind Turbine Using a 12-Sectors DTC,” *WEVJ*, vol. 13, no. 7, p. 123, 2022, doi: 10.3390/wevj13070123.
[16] A. Mujcinagic, M. Kusljugic, and J. Osmic, “Frequency Response Metrics of an Interconnected Power System,” in *2019 54th International Universities Power Engineering Conference (UPEC)*, Bucharest, Romania, 2019, pp. 1–5.
[17] S. Harasis and Y. Sozer, “Improved Transient Frequency Stabilization of Grid Feeding Distributed Generation Systems Using Active Damping Control,” in *2019 IEEE Energy Conversion Congress and Exposition (ECCE)*, Baltimore, MD, USA, 2019, pp. 4324–4330.
[18] A. Fernández-Guillamón, A. Vigueras-Rodríguez, and Á. Molina-García, “Analysis of power system inertia estimation in high wind power plant integration scenarios,” *IET Renewable Power Generation*, vol. 13, no. 15, pp. 2807–2816, 2019, doi: 10.1049/iet-rpg.2019.0220.
[19] B. Tan, J. Zhao, M. Netto, V. Krishnan, V. Terzija, and Y. Zhang, “Power system inertia estimation: Review of methods and the impacts of converter-interfaced generations,” *International Journal of Electrical Power & Energy Systems*, vol. 134, p. 107362, 2022, doi: 10.1016/j.ijepes.2021.107362.
[20] Y. Mitsugi, H. Hashiguchi, T. Shigemasa, Y. Ota, T. Terazono, and T. Nakajima, “Control Hardware-in-the-Loop Simulation on Fast Frequency Response of Battery Energy Storage System Equipped With Advanced Frequency Detection Algorithm,” *IEEE Trans. on Ind. Applicat.*, vol. 57, no. 6, pp. 5541–5551, 2021, doi: 10.1109/TIA.2021.3107223.
[21] X. Pan, B. Zhou, H. Gao, and Y. Wang, “Modeling of aggregated wind power generation’s active participation to system frequency regulation,” in *2019 IEEE 3rd Conference on Energy Internet and Energy System Integration (EI2)*, Changsha, China, 2019, pp. 176–181.
[22] H. T. Nguyen, G. Yang, A. H. Nielsen, and P. H. Jensen, “Frequency stability enhancement for low inertia systems using synthetic inertia of wind power,” in *2017 IEEE Power & Energy Society General Meeting*, Chicago, IL, 2017, pp. 1–5.
[23] C. Cieslak and L. Grunwald, “Modelling Synthetic Inertia of Wind Turbines for Dynamic Power System Stability Studies,” in *2019 54th International Universities Power Engineering Conference (UPEC)*, Bucharest, Romania, 2019, pp. 1–6.
[24] A. Jain, N. P. Padhy, and M. K. Pathak, “Quantification of inertia contribution from non-conventional sources in AC Microgrid,” in *2022 IEEE International Conference on Power Electronics, Smart Grid, and Renewable Energy (PESGRE)*, Trivandrum, India, 2022, pp. 1–6.
[25] R. Wu, W. Li, Z. Li, H. Zeng, N. Zou, and Z. Wang, “Quantification Method for

Inertia Heterogeneity of Power System Considering Node Coupling," in *2022 IEEE 2nd International Conference on Electronic Technology, Communication and Information (ICETCI)*, Changchun, China, 2022, pp. 1–6.
[26] D. Ochoa and S. Martinez, "Fast-Frequency Response Provided by DFIG-Wind Turbines and its Impact on the Grid," *IEEE Trans. Power Syst.*, vol. 32, no. 5, pp. 4002–4011, 2017, doi: 10.1109/TPWRS.2016.2636374.
[27] Y. Zhang, F. Qi, Y. He, B. Wang, and D. Yang, "Synchrophasor data-based inertia estimation for regional grids in interconnected power systems," *Front. Energy Res.*, vol. 10, 2022, doi: 10.3389/fenrg.2022.989430.
[28] A. Femandez-Guillamon, A. Molina-Garcia, A. Vigueras-Rodriguez, and E. GOmez-Lazaro, "Frequency Response and Inertia Analysis in Power Systems with High Wind Energy Integration," in *2019 International Conference on Clean Electrical Power (ICCEP)*, Otranto, Italy, 2019, pp. 388–393.
[29] R. Fu, X. Wang, Y. Zhang, and L. Li, "Inertial and Primary Frequency Response of PLL Synchronized VSC Interfaced Energy Resources," *IEEE Trans. Power Syst.*, vol. 37, no. 4, pp. 2998–3013, 2022, doi: 10.1109/TPWRS.2021.3130343.
[30] D. A. Kez, A. M. Foley, and D. J. Morrow, "Analysis of Fast Frequency Response Allocations in Power Systems With High System Non-Synchronous Penetrations," *IEEE Trans. on Ind. Applicat.*, vol. 58, no. 3, pp. 3087–3101, 2022, doi: 10.1109/TIA.2022.3160997.
[31] L. Ibarra, A. Rosales, P. Ponce, A. Molina, and R. Ayyanar, "Overview of Real-Time Simulation as a Supporting Effort to Smart-Grid Attainment," *Energies*, vol. 10, no. 6, p. 817, 2017, doi: 10.3390/en10060817.
[32] M. C. Magro, M. Giannettoni, P. Pinceti, and M. Vanti, "Real time simulator for Microgrids," *Electric Power Systems Research*, vol. 160, pp. 381–396, 2018, doi: 10.1016/j.epsr.2018.03.018.
[33] C. Keerthisinghe and D. S. Kirschen, "1 Real-Time Digital Simulation of Microgrid Control Strategies," in *2020 IEEE Power & Energy Society Innovative Smart Grid Technologies Conference (ISGT)*, Washington, DC, USA, 2020, pp. 1–5.
[34] M. Farzinfar, M. Jazaeri, N.-K. C. Nair, and F. Razavi, "Stability evaluation of Microgrid using real-time simulation," in *2014 Australasian Universities Power Engineering Conference (AUPEC)*, Perth, Australia, 2014, pp. 1–6.
[35] R. AhmadiAhangar, A. Rosin, A. N. Niaki, I. Palu, and T. Korõtko, "A review on real-time simulation and analysis methods of Microgrids," *Int Trans Electr Energ Syst*, vol. 29, no. 11, 2019, doi: 10.1002/2050-7038.12106.

Appendix A. Derivation of Swing Equation roots for inertia evaluation

Considering the swing equation after multiplying both sides by the angular speed, the following equation can be obtained.

$$P_{tran} = P_{in} - P_{out} = J\omega\frac{d^2\Delta\delta}{dt} + B\frac{d\Delta\delta}{dt} = J\omega\frac{d\Delta\omega}{dt} + B\Delta\omega \quad (A.1)$$

multiplying both sides by $\frac{\omega}{2}$yields:

$$(P_{in} - P_{out})\frac{\omega}{2} = \frac{J\omega^2}{2}\frac{d^2\Delta\delta}{dt^2} + \frac{\omega}{2}B\frac{d\Delta\delta}{dt} \quad (A.2)$$

dividing by KVA to get the values of H and D from the pu form

$$(P_{in} - P_{out})\frac{\omega}{2} = H\frac{d^2\Delta\delta}{dt^2} + \mathrm{D}\frac{d\Delta\delta}{dt} \quad (A.3)$$

where, the damping coefficient D= $\frac{\omega}{2S}B$ and the inertia coefficient $H = \frac{J\omega^2}{2S}$.(A.3) can be rearranged as:

$$P_{\mathrm{tran}_{pu}} = \frac{2H}{\omega}\frac{d^2\Delta\delta}{dt^2} + \frac{2D}{\omega}\frac{d\Delta\delta}{dt}\ \mathrm{PU} \quad (A.4)$$

Now linearizing (A.4) by considering the following:

$\mathrm{Sin}\,(\delta + \Delta)$=sin$\delta cos\Delta\delta + cos\delta sin\Delta\delta$ and since $\delta\Delta$ is small

$\cos\delta\Delta = 1\ and\ \sin\delta\Delta = \Delta\delta$, the folowing can ne obtained.

$$P_{out} = P_{out} + \Delta P_{out} = \frac{EV}{X}\{sin\delta + \delta\cos\delta\} \quad (A.5)$$

Plug (A.5) into (A.4) and eliminating the steady state yields:

$$\ddot{\Delta\delta} + \frac{D}{2H}\dot{\Delta\delta} + \frac{\frac{EVcos\delta}{X}}{2H/\omega}\Delta\delta = \Delta P_{out} \quad (A.6)$$

Taking Laplace transform and rearranging yields:

$$s^2\Delta\delta(s) + \frac{D\Delta\delta(s)}{2H/\omega}s + \frac{\frac{EVcos\delta}{X}}{2H/\omega}\Delta\delta(s) = \Delta P_{out}(s) \quad (A.7)$$

Further simplification yields:

$$s^2 + \frac{D}{2H}s + \frac{EVcos\delta}{X}\frac{\omega}{2H} = 0 \quad (A.8)$$

So, the denominator of (A.8) which is for the transfer function $\frac{\Delta P_{out}(s)}{\Delta\delta(s)}$is :

$$\mathrm{S}_{1,2} = \frac{-D}{4H} \mp \sqrt{(\frac{D}{4H})^2 - \frac{EVcos\delta}{X}\frac{\omega}{2H}} \quad (A.9)$$

Appendix B. Experiment source csv log files

"*.CSV" files of the three-phase voltage, current, active power of the Microgrid nodes at all operating conditions are attached to the report.

Disclaimer

This document contains material, which is copyrighted by the authors and may not be reproduced or copied without permission.

The commercial use of any information in this document may require a licence from the proprietor of that information.

Neither the Lab Access User Group as a whole, nor any single person warrant that the information contained in this document is capable of use, nor that the use of such information is free from risk. Neither the Lab Access User Group as a whole, nor any single person accepts any liability for loss or damage suffered by any person using the information.

This document does not represent the opinion of the European Community, and the European Community is not responsible for any use that might be made of its content.

Copyright Notice